ACS APPLIED MATERIALS & INTERFACES

Research Article

www.acsami.org

Nongassing Long-Lasting Electro-osmotic Pump with Polyaniline-wrapped Aminated Graphene Electrodes

Rudra Kumar, Kousar Jahan, Rajaram K. Nagarale,* and Ashutosh Sharma*

Department of Chemical Engineering, Indian Institute of Technology, Kanpur 208016, India

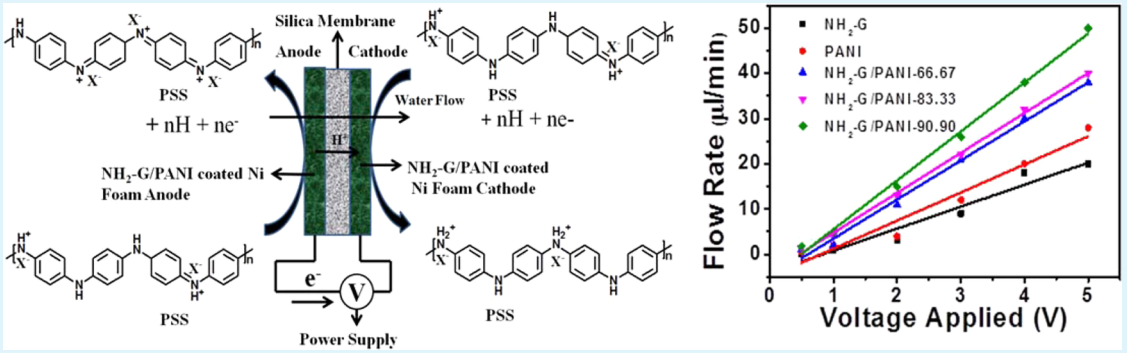

ABSTRACT: An efficient nongassing electro-osmotic pump (EOP) with long-lasting electrodes and exceptionally stable operation is developed by using novel flow-through polyaniline (PANI)-wrapped aminated graphene (NH_2-G) electrodes. The NH_2-G/PANI electrode combines the excellent oxidation/reduction capacity of PANI with the exceptional conductivity and inertness of NH_2-G. The flow rate varies linearly with voltage but is highly dependent on the electrode composition. The flow rates at a potential of 5 V for pristine NH_2-G and PANI electrodes are 71 and 100 μL min^{-1} cm^{-2}, respectively, which increase substantially by the use of NH_2-G/PANI electrode. It increased from 125 to 182 μL min^{-1} cm^{-2} as the fraction of aniline increased from 66.63 to 90.90%. The maximum flux obtained is 40 μL min^{-1} V^{-1} cm^{-2} with NH_2-G/PANI-90.9 electrodes. The assembled EOP remained exceptionally stable until the electrode columbic capacity was fully utilized. The prototype shown here delivered 8.0 μL/min at a constant applied voltage of 2 V for over 7 h of continuous operation. The best EOP produces a maximum stall pressure of 3.5 kPa at 3 V. These characteristics make it suitable for a variety of microfluidic/device applications.

KEYWORDS: *electro-osmotic pump, microfluidics, functionalized graphene, polyaniline, silica membrane*

INTRODUCTION

The development of high-performance, nongassing, long-lasting electrodes for electro-osmotic pumps (EOPs) is currently of much interest,[1−7] owing to a plethora of important applications in drug delivery,[1,8,9] microfluidics,[10] compact bioanalytical systems,[11] lab on a chip assays,[11−13] and device actuation.[14] The first nongassing electrode reported was based on Ag/AgCl, followed by Ag/Ag_2O,[1] poly(3,4-ethylenedioxythiophene) (PEDOT)[5] and functional carbon[3] in recent years. Here, we demonstrate for the first time the use of flow-through nickel-foam-supported polyaniline (PANI)-wrapped aminated graphene (NH_2-G) composite as nongassing, long lasting and reversible electrodes for EOPs. The hybrid electrodes combine the excellent proton transport associated oxidation/reduction property of PANI with exceptional conductivity and inertness of NH_2-G. The flow of the pump starts at 0.5 V, the potential well below the thermodynamic potential of water electrolysis (1.23 V), and hence, no generation of hydrogen and oxygen was occurs on respective electrodes.

The factors that explain the attractiveness of EOPs are the ease of preparation (through sandwich assembly), lack of moving parts, easy integration into miniaturized devices, and delivery of pulse-free flows in the nanoliter range. They also maintain the pumped solutions at specific and constant flow rates with respect to the potential and current applied, allowing the coulometric volume of the solution to be measured.

The work on developing nongassing electrode is started in 1977 by Luft, Kuhl, and Richter.[6] The very small flow rate of 0.7 μL min^{-1} and high current density of 1 mA cm^{-2} limited its further development. Recently, we have successfully demonstrated nongassing EOP with consumable Ag/Ag_2O electrodes having 130 μL min^{-1} V^{-1} cm^{-2} electro-osmotic flux.[1] The use of the quinone/hydroquinone redox couple generated by oxygen plasma treatment of a carbon-paper electrode has been reported.[3] The redox active alizarin dye electrode in EOP resulted in 27 ± 1.5 μL min^{-1} V^{-1} cm^{-2} electro-osmotic flux at a silica frit zeta potential of −52 mV.[3] The extremely high performance EOPs with a 15 nm thick porous nanocrystalline silicon membrane is reported with voltages as low as 250 mV and electro-osmotic flux of 2600 μL min^{-1} V^{-1} cm^{-2}.[7]

The use of graphene-based electrode materials[15−20] and their composites with conducting polymers[21−26] show interesting

Received: October 1, 2014
Accepted: December 5, 2014
Published: December 5, 2014

   dx.doi.org/10.1021/am506766e | ACS Appl. Mater. Interfaces 2015, 7, 593−601

synergies that have proved advantageous in supercapacitors,[21] nanoelectronics,[22] lithium ion batteries,[22] dye sensitized solar cells,[23,24] microbial fuel cells,[25] gas sensing,[26] transparent electrodes,[27] anticorrosion coating,[28] and biocompatible free-standing electrodes.[29] The redox conducting polymers are associated with proton transfer in oxidation/reduction processes and could thus have potential in EOP electrodes notwithstanding the challenges posed by their increased resistance during the redox processes, for example, fully oxidized pernigraniline or reduced leucoemeraldine forms of PANI is poor conducting. However, there is very limited work on the use of conducting polymers as a nongassing electrode in EOPs.[5] Use of appropriately functionalized graphene coupled with a redox conducting polymer may further circumvent the limitations on the conductivity of the polymer. Here, we report the use of nickel-foam-supported neat PANI, NH_2-G- and NH_2-G-wrapped PANI composite as nongassing electrode materials for electro-osmotic pumping. Indeed, the performance of composite electrodes far exceeds the pristine PANI- and NH_2-G-based electrodes and compares favorably with the best nongassing electrodes. We also note that the overall performance of an EOP depends not only on electrodes but also on the permeability and zeta potential of the proton conducting membrane sandwiched between the electrodes. Several exceptionally thin and porous membranes, such as ultrathin porous silica, have been developed recently.[7] However, the focus here is on the development of efficient electrodes, which are demonstrated with more commonly deployed relatively thick colloidal silica frits,[30] without an effort on the optimization of the membrane.

EXPERIMETAL SECTION

Materials. Flake graphite (45 μm) was purchased from Alfa Aesar. Potassium permanganate, sodium nitrate, H_2SO_4, aniline, potassium dichromate, ethylene glycol, and liquor ammonia were purchased from Fisher Scientific. Polystyrene sulfonic acid and Nafion (5 wt % in a 1:1 solution of water and lower aliphatic alcohol) were purchased from Sigma-Aldrich. Nickel foam was purchased from MTI Corporation. All the reagents were analytical grade and used without further purification.

Synthesis of Graphene Oxide. Graphite oxide (GO) was synthesized using the modified Hummers method[31] reported in the literature. Briefly, 1 g of preoxidized flake graphite was mixed for 10 min at 0 °C in an ice bath with 1 g of sodium nitrate and 46 mL of concentrated H_2SO_4. Then, 6 g of $KMnO_4$ was slowly added as the temperature was maintained at 20 °C. After the solution was properly mixed, it was transferred to a water bath to maintain the solution temperature at 35 ± 5 °C and stirred for about 2 h, leading to the formation of a thick paste. After the addition of g 80 mL of deionized (DI) water, the solution was stirred for 30 min while the temperature was raised to 95 °C, and then 200 mL of DI water and 6 mL of 30% H_2O_2 were added. After adding all the H_2O_2, the solution changed color, from dark brown to yellow. The warm solution obtained was filtered and then washed with 30% concentrated HCl solution to remove any sulfate present in the graphite oxide solution. The resulting filter cake was redispersed in 200 mL of DI water by mechanical stirring. Centrifugation was carried out at a low rotation speed (1000 rpm) for 2 min to remove the unexfoliated graphite. This procedure was repeated two to three times to remove all visible particles. The supernatant obtained was further centrifuged at 8000 rpm for 15 min to remove the small GO flakes and water-soluble byproducts. The precipitate from high-speed centrifugation was collected and vacuum-dried overnight at 60 °C in a vacuum oven to obtain solid graphite oxide.

Synthesis of Amine-Functionalized Graphene (NH_2-G). Amine-modified GO was prepared as reported.[32] In brief, 100 mg of GO was dispersed in 40 mL of ethylene glycol by ultrasonication. After complete exfoliation of the GO, 1 mL of ammonia−water was added. This mixture was then transferred into a hydrothermal reactor and kept at 180 °C for 10 h. After the reaction was completed, the black precipitate was filtered and washed with DI water three times. Finally, the product was dried overnight in a vacuum oven.

Synthesis of Polyaniline. Polyaniline was chemically synthesized by rapid mixing. First, 1 mL of aniline was dissolved in a mixture of 20 mL DI water and 10 mL concentrated H_2SO_4 solution. Polystyrene sulfonic acid (7 mL with 18 wt % H_2O) was added to the homogenized solution. The mixture was then stirred vigorously at room temperature while 1 mL of 0.3 M potassium dichromate ($K_2Cr_2O_7$) solution was added dropwise. The polymerization of aniline initiated instantaneously. The characteristic green color of PANI emeraldine salt was observed after the addition of potassium dichromate. The mixture was set aside for 5 h for the polyaniline to precipitate. The resulting polymer was collected by centrifugation and washed with distilled water until free of sulfate ions.

Synthesis of NH_2-G/polyaniline Composites. NH_2-G/Polyaniline composites were prepared by in situ polymerization of aniline in a suspension of NH_2-G in an acidic medium. Typically, 100 mg of NH_2-G was dispersed in 20 mL of distilled water using a probe sonicator to prevent the graphene sheets from restacking. Then, 10 mL of concentrated H_2SO_4 was added to the dispersion followed by the required amount of aniline. After complete mixing, 7 mL polystyrene sulfonic acid was added. The mixture was stirred continuously at room temperature, and 1 mL of 0.3 M $K_2Cr_2O_7$ was added dropwise to initiate the polymerization, which was carried out for 5 h. The PANI-wrapped NH_2-G precipitates were collected by centrifugation and washed with distilled water until they were free of sulfate. Five different samples were synthesized by changing the weight fraction of aniline in the reaction mixture, namely 0, 66.7, 83.3, 90.9, and 100 wt % aniline. The samples are named NH_2-G/PANI-X where X indicates the weight percentage of aniline in the reaction mixture.

Silica Membrane and Electrode Preparation and Pump Assembly. The silica membrane was prepared as reported previously.[2] The flow-through electrodes were prepared by dip coating NH_2-G/PANI paste on nickel foam. The paste was prepared by dispersing 400 mg of NH_2-G/PANI composite in 8 mL of isopropyl alcohol and 2 mL of Nafion solution (5 wt % in a water−alcohol mixture). Before coating, the nickel foam was cleaned with 0.1 M hydrochloric acid and thoroughly washed with DI water. The coated nickel foam was dried in oven at 100 °C for 1 h and used to prepare 8 mm diameter discs used to assemble the pump as reported previously.[1] For comparison, electrodes were prepared similarly with neat NH_2-G and PANI.

General Characterization. The structural and morphological characterization of neat NH_2-G, PANI, and the NH_2-G/PANI composites was performed by field emission scanning electron microscopy (FESEM, ZEISS Supra 40VP, Jena, Germany), and energy dispersive X-ray spectroscopy (EDX) with elemental mapping using an Oxford Instruments EDS system attached to the FESEM machine. Crystal structures were obtained by X-ray diffraction (XRD) (PANalytical, Dresden, Germany) of Cu Kα radiation (λ = 1.5406 Å) from 5 to 80° at a scanning speed of 2° per minute. Raman spectroscopy (WITec alpha300 R, Germany) was performed in the frequency range of 400−3000 cm^{-1} with a 514 nm laser source to identify the stretching modes of polyamine and carbon. UV−visible spectra were measured for wavelengths from 200−800 nm using a UV−visible spectrophotometer (Varian Cary 50 Bio, Palo Alto, CA). Fourier transform infrared spectra (FTIR) were recorded in the frequency range from 400−4000 cm^{-1}. Atomic force microscopy (Agilent Pico View 1.14.2, Santa Clara, CA) measurements were performed in noncontact mode. The samples were prepared on the surface of a mica sheet. The electrical conductivity was measured using a four-point conductivity probe (SES Instruments, Roorkee, Uttarakhand, India) attached to a Keithley current source and voltmeter for all samples; bare carbon paper, PANI, NH_2-G and NH_2-G/PANI composite deposited on carbon paper. The flow was measured using a custom-built equipment. A constant potential was applied using a CHI 760E electrochemical analyzer (CH Instruments, Austin, TX).

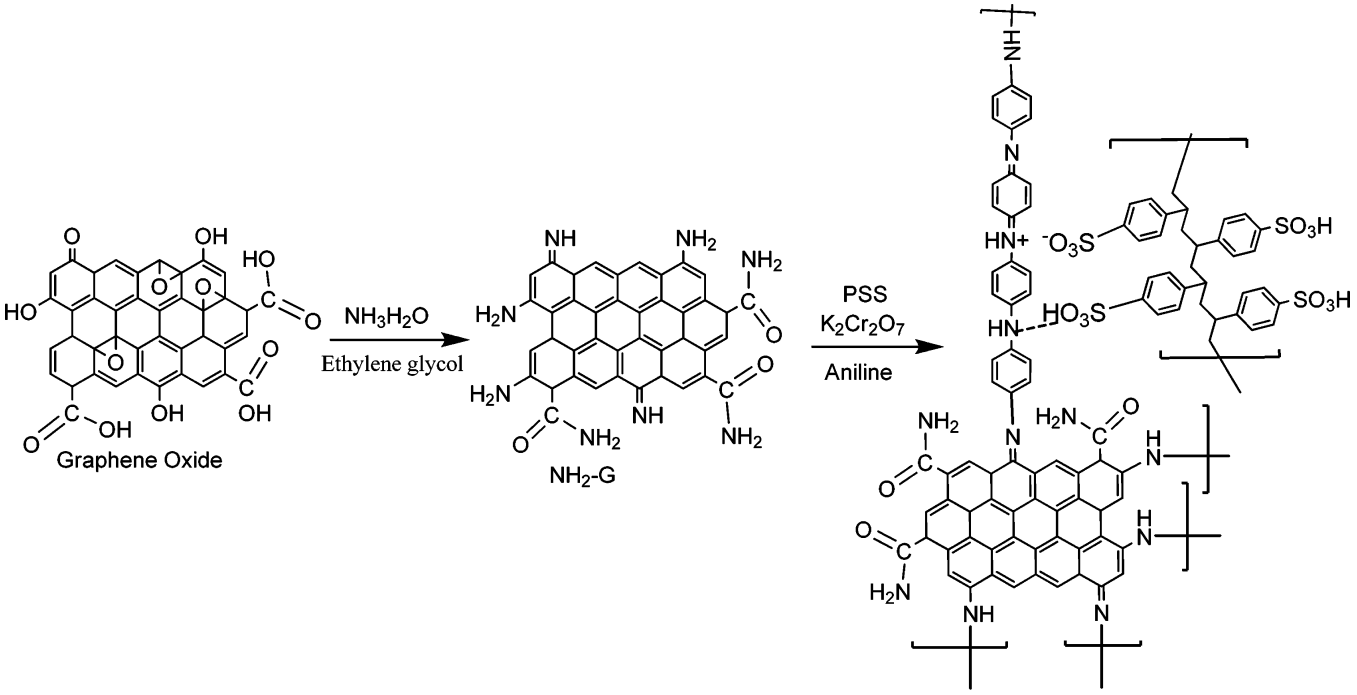

Figure 1. Schematics of the synthesis of PANI wrapped aminated graphene by polymerization of aniline in the presence of PSS and $K_2Cr_2O_7$ as catalyst.

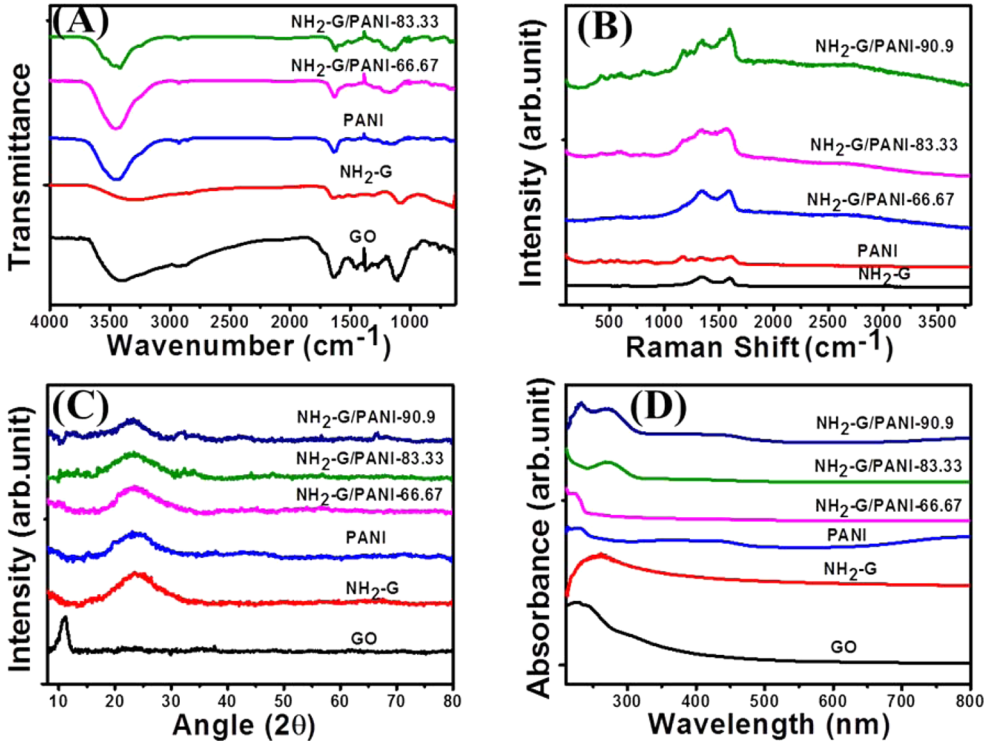

Figure 2. Characterizations of neat NH_2-G, PANI, and NH_2-G/PANI composites. (A) FTIR spectra were recorded in powder form in frequency range 400−4000 cm^{-1}. (B) Raman spectra were recorded in powder form in frequency range 100−3750 cm^{-1}. (C) Powder XRD was recoded at 2° min^{-1} scan rate using Cu Kα radiation (λ = 1.5406 Å). (D) UV−visible spectra were recorded after dispersing in proper solvent. The solvent used were water for GO, NH_2-G, PANI and isopropyl alcohol for NH_2-G/PANI composite. The spectra were plot after baseline corrections.

RESULTS AND DISCUSSION

Preparation of NH_2-G/PANI Composites. The electrode material, PANI-wrapped aminated graphene (NH_2-G/PANI) was prepared by in situ polymerization of aniline with potassium dichromate in the presence of aminated graphene (NH_2-G) and polystyrene sulfonic acid. A schematic of the preparation is depicted in Figure 1. The NH_2-G was prepared by hydrothermal treatment of GO in the presence of aqueous ammonia and ethylene glycol. In ethylene glycol, a reducing environment, ammonia reacts readily with oxygen functional groups such as epoxide, hydroxyl, and carboxyl by nucleophilic substitution, and is converted into amide- and amine-functionalized GO.[32] The

dx.doi.org/10.1021/am506766e | ACS Appl. Mater. Interfaces 2015, 7, 593−601

presence of these functional groups was confirmed by recoding FTIR spectra of neat GO and of NH_2-G, as shown in Figure 2A. The presence of vibrational absorbance troughs in the spectrum proves the existence of the different functional groups through their signature wavenumbers. The peaks observed at 3434, 1723, and 1628 cm^{-1} correspond to the hydrogen bonds associated with O−H groups, the C═O bonds of carboxylic acid, and the carbonyl moiety of GO, respectively. The C−O bonds are observed at a vibrational frequency of 1224 cm^{-1}, while the signal for the epoxy group is at 655 cm^{-1}. Following NH_2 modification, the peaks at 3434, 1723, and 1628 cm^{-1} decay significantly highlighting the reduction and amine functionalization of the GO sheets.[32] The absorption peaks at 3300−3500 cm^{-1} arise from the stretching of the N−H bonds of the amine groups, while the peak at 1580 cm^{-1} is assigned to in-plane N−H stretching.

The NH_2-G/PANI composite was obtained by oxidative polymerization of PANI in an aqueous dispersion of NH_2-G. The presence of styrene sulfonic acid and sulfuric acid and the constant stirring at about 1000 rpm facilitated the wrapping of NH_2-G with PANI and prevented their agglomeration. The wrapping of NH_2-G with PANI was confirmed by FTIR (Figure 2A). The peak observed for PANI at 1481 cm^{-1} corresponds to the C═C vibration of the quinoid and benzene ring deformation, while the peak at 1293 cm^{-1} is assigned to C−N stretching in the benzoid ring. The range of peaks from 1250−1020 cm^{-1} arise from C−N stretching in aromatic amines.[33] The peaks at 815 and 1637 cm^{-1} come from the sulfonic acid groups present in the composite and from N−H bending in primary amine, respectively.

Further confirmation of the formation of NH_2-G, PANI, and NH_2-G/PANI composite was provided by Raman spectroscopy, which is a versatile technique used notably to identify carbon based materials.[29] Figure 2B shows the Raman spectra of neat NH_2-G, PANI, and of the NH_2-G/PANI composites. The peaks observed at 1344 and 1590 cm^{-1} for neat NH_2-G are assigned to the D and G bands, respectively. The D band comes from disordered carbon phase resulting from the conversion of sp^2 hybridized carbon to sp^3 hybridized carbon, while the G band arises from the in-plane stretching of the sp^2 hybridized carbon in graphite.[34,35] The intensity of the D band was higher than that of the G band, confirming the disordering of graphite stemming from the formation of amine functional groups.[36] The presence of PANI is also evidenced in the Raman spectra. The peak observed at 1160 cm^{-1} is assigned to the C−H stretching vibration of the aniline ring. The N−H and C−H bending vibrations are observed at 1504 and 1172 cm^{-1}, respectively. The peaks observed at 812, 720, 638, and 572 cm^{-1} are assigned to bipolaronic quinoid ring vibrations. The peak at 512 cm^{-1} is assigned to the polaronic amine vibration, and the one at 406 cm^{-1} is assigned to polaronic C−N−C torsion.[26] The peak observed at 1590 cm^{-1} in the spectrum from the NH2-G/PANI composite sample is broader and wider than in the NH_2-G spectrum. This is attributed to the successful incorporation of polyaniline nanostructures between the graphene sheets.[24]

Powder XRD further supported the formation of NH_2-G, PANI, and NH_2-G/PANI, as shown in Figure 2C In this figure, an intense peak is clearly observed in the spectrum of neat GO at a 2θ value of 11.1°. The peak is assigned to the (001) plane with and interlayer spacing between the graphene oxide sheets of ~0.79 nm. The formation of NH_2-G by solvothermal treatment of GO with ammonia and ethylene glycol results in a shifting of the peaks. The peak at 2θ = 23.64° with an interlayer spacing of d = 0.37 confirms the formation of NH_2-G. The broadness of the peak is due to the poor stacking of modified graphene sheets. The spectrum of neat PANI exhibits a peak at 2θ = 23.4° with an interlayer spacing of d = 0.35 nm. The wrapping of PANI over the graphene sheets decreases the 2θ value because of an increase in the interlayer spacing of about 0.39 nm. Additional evidence of the wrapping of PANI over the graphene sheets was obtained by recording UV−visible spectra, and SEM and AFM images.

Figure 2D shows the UV−visible spectra of neat GO, NH_2-G, and of the NH_2-G/PANI composites. The absorption peak for GO is observed at 232 nm corresponding to the $\pi-\pi^*$ transition of the C═C bond. After the reaction with ammonia, the absorption peak shows a red shift and is observed at 260 nm (corresponding to NH_2-G). The peaks observed at 352 and 800 nm highlight the formation of conducting PANI.[33−37] The NH_2-G/PANI composite shows absorption at 270 nm and a broad peak at 434 nm.

Morphology and Structure of PANI and the NH_2-G/PANI Composites. Figure 3A shows SEM images of neat NH_2-G, PANI, and of the NH_2-G/PANI composites prepared with different PANI loadings by varying the aniline concentration.

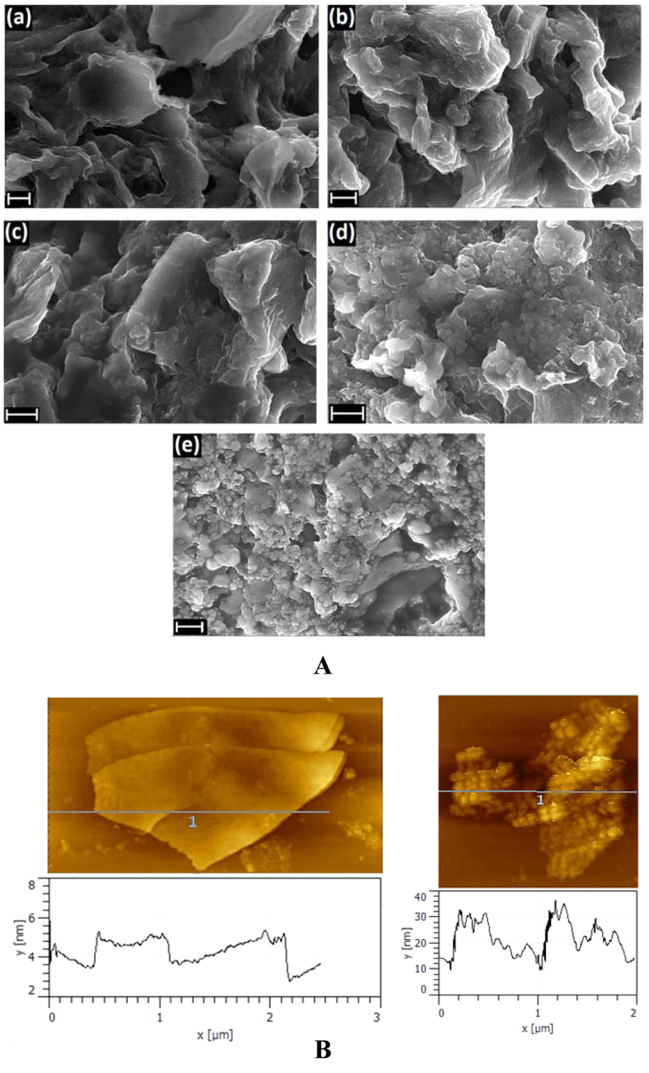

Figure 3. (A) SEM images of NH_2-G and NH_2-G/PANI composite. (a) Neat NH_2-G, (b) NH_2-G/PANI-66.7, (c) NH_2-G/PANI-83.3, (d) NH_2-G/PANI-90.9, (e) neat PANI, scale bar (1 μm). (B) AFM images of (right) neat NH_2-G and (left) NH_2-G/PANI-90.9 with corresponding height profile.

dx.doi.org/10.1021/am506766e | ACS Appl. Mater. Interfaces 2015, 7, 593−601

The presence of sheet-like NH_2-G structures is clearly visible in the images. The wrapping of PANI over NH_2-G is observed in Figure 3A,b−d. As the concentration of aniline is increased in the polymerizing solution, the surface morphology of NH_2-G also changes. At lower concentrations of aniline, (i.e., for NH_2-G/PANI-66.7), creased agglomerated sheets are observed, while at higher concentrations (i.e., for NH_2-G/PANI-90.9), a high extent of agglomeration can be seen with irregular shaped PANI particles on the NH_2-G surface. For neat PANI, dense irregular shaped particles are observed (Figure 3A,e.

AFM imaging in noncontact mode was carried out to validate the wrapping of PANI over NH_2-G. Figure 3B shows the height profiles of neat NH_2-G and of the NH_2-G/PANI-90.9 composite. The creased morphology of the NH_2-G sheets is observed with height profiles of 3−5 nm. The image taken of NH_2-G/PANI-90.1 shows small evenly distributed spherical agglomerated particles of PANI over the NH_2-G sheets that are 20−25 nm in height.

The extended diiminoquinone−diaminobenzene type bonding of PANI with NH_2-G should enhance the electrical conductivity because of efficient electron hopping, while the presence of PSS provides hydrophilicity and proton swapping. This hypothesis was scrutinized by measuring the conductivity of the composite materials. Figure 4 shows the current−voltage (I−V) curves measured for neat NH_2-G, PANI, and the NH_2-G/PANI composites using a four-point probe at room temperature. The specimens for measurements were prepared by dip coating electrode active materials on porous carbon paper (Toray Carbon). The linear dependence of the current on the applied voltage in Figure 4 reveals the conductive nature of the materials. Conductivity was calculated using the relation $\rho = 4.52 \times (V/I) \times t$, where ρ, V, I and t are the resistivity, voltage, current, and thickness of the electrode, respectively. The thickness of the specimens is taken as the whole of carbon paper plus deposited composites material. The composite material cannot be isolated from the carbon substrate because some material penetrates into the pores of the carbon paper. This introduces some uncertainty in the calculation of the thickness of the deposited material. The plain carbon paper had a conductivity of 102.5 S/cm. When coated with NH_2-G and neat PANI, its conductivity was found to be ∼94.6 S/cm and 81.6 S/cm, respectively. The reduction in conductivity of the carbon paper coated with NH_2-G or with PANI is due to the higher resistivity of these materials. On the other hand, an increase in conductivity was found by coating composite material. The obtained conductivity was 84.7, 100.7, and 109.2 S/cm for NH_2-G/PANI-66.67, NH_2-G/PANI-83.33, and NH_2-G/PANI-90.9, respectively. It indicates an increase in the conductivity of the composites material with an increase in the weight fraction of aniline. The sample, NH_2-G/PANI-90.9 with a high weight fraction of aniline, also has the highest conductivity. The high conductivity is due to the presence of graphene sheets and extended covalent imine bonding between PANI and NH_2-G, which facilitates proton hopping. Further, the change in porosity and morphology of the composite material may have also contributed to increase in conductivity. The presence of PSS allows hydrophilicity and proton swapping.

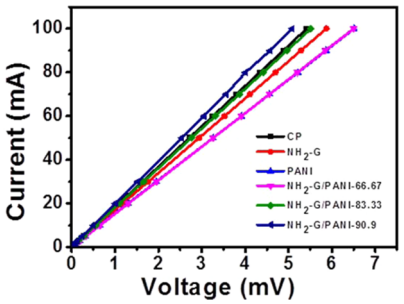

Figure 4. I−V curves for the Neat NH_2-G, PANI, and NH_2-G/PANI-composites measured at room temperature after dip coating on Toray carbon paper with paste of NH_2-G, PANI, and NH_2-G/PANI composites.

Pump Performance. Electro-osmotic pumps were assembled with a sandwich structure, with flow-through electrodes made from neat NH_2-G, PANI, NH_2-G/PANI-66.67, NH_2-G/PANI-83.33, and NH_2-G/PANI-90.9, after coating the corresponding paste on nickel foam and silica frit. Figure 5A shows images obtained before and after coating the nickel foam with NH_2-G/PANI-90.9. The electro-active coating was uniform and firmly attached to the nickel foam surface. We found that, even after several days of immersion in distilled water, the coating did not detach from the surface. The pump assembly was made by sandwiching a silica frit between the prepared flow-through nickel-foam-coated electrodes (Figure 5B). The frit was synthesized by treating phosphosilicate pallet made from 1 μm diameter monodispers silica particles at 700 °C for 4 h as discussed elsewhere.[1] The frit was ∼1 mm thick, and the zeta potential of the constituting particles measured before making the frit was −34 mV.

The miniaturized pump developed here had an active membrane/frit diameter of 0.28 cm^2. The pumping performance was tested by operating the EOP at a constant potential. The dependence of the flow rate on the applied potential is shown in Figure 6A for electrodes prepared using neat NH_2-G, PANI, and different NH_2-G/PANI composites. For all these electrodes, the flow rate is linearly dependent on the applied voltage. The lowest flow-inducing potential was 0.5 V. This voltage is well below the thermodynamic potential required to electrolyze water, which is 1.23 V, and the potential of 2.5 V measured for gassing platinum electrodes.[1] From Figure 6A, it is evident that the flow rate increases with the PANI content in the NH_2-G/PANI composites for distilled water. The presence of added salt or buffer solution decreases the flow rate. However, we can run at very low concentration of electrolyte solutions of different salts and acid. It may, however, be noted that water is only a "working fluid", that is, the pressure generated by the pump can be used to push any other liquid. The maximum electro-osmotic flux for distilled water (i.e., the flux per unit applied voltage) obtained from slopes in Figure 6A is 40.4 $\mu L\ min^{-1}\ cm^{-2}\ V^{-1}$ for the NH_2-G/PANI-90.9 composition, and the lowest, 19.0 $\mu L\ min^{-1}\ cm^{-2}\ V^{-1}$ for neat NH_2-G. With a neat PANI electrode, the electro-osmotic flux was 24.3 $\mu L\ min^{-1}\ cm^{-2}\ V^{-1}$. The higher fluxes afforded by the composite electrodes compared with those prepared with neat NH_2-G or PANI may be due to the presence of comparatively higher conductivity accompanying redox moieties by PANI wrapped graphene sheet and efficient hopping of protons through the extended covalent diiminoquinone−diaminobenzene bonding between PANI and NH_2-G. Furthermore, the presence of PSS and Nafion in the composite electrodes makes them hydrophilic and promotes proton swapping. This performance is superior to that of an EOP assembled with PEDOT blended PSS-based electrodes.[5] The flux is also considerably larger than those observed in EOPs employing high-voltage porous glass[38] and ion-exchange membranes.[39] However, it is lower than the fluxes reported for

dx.doi.org/10.1021/am506766e | ACS Appl. Mater. Interfaces 2015, 7, 593−601

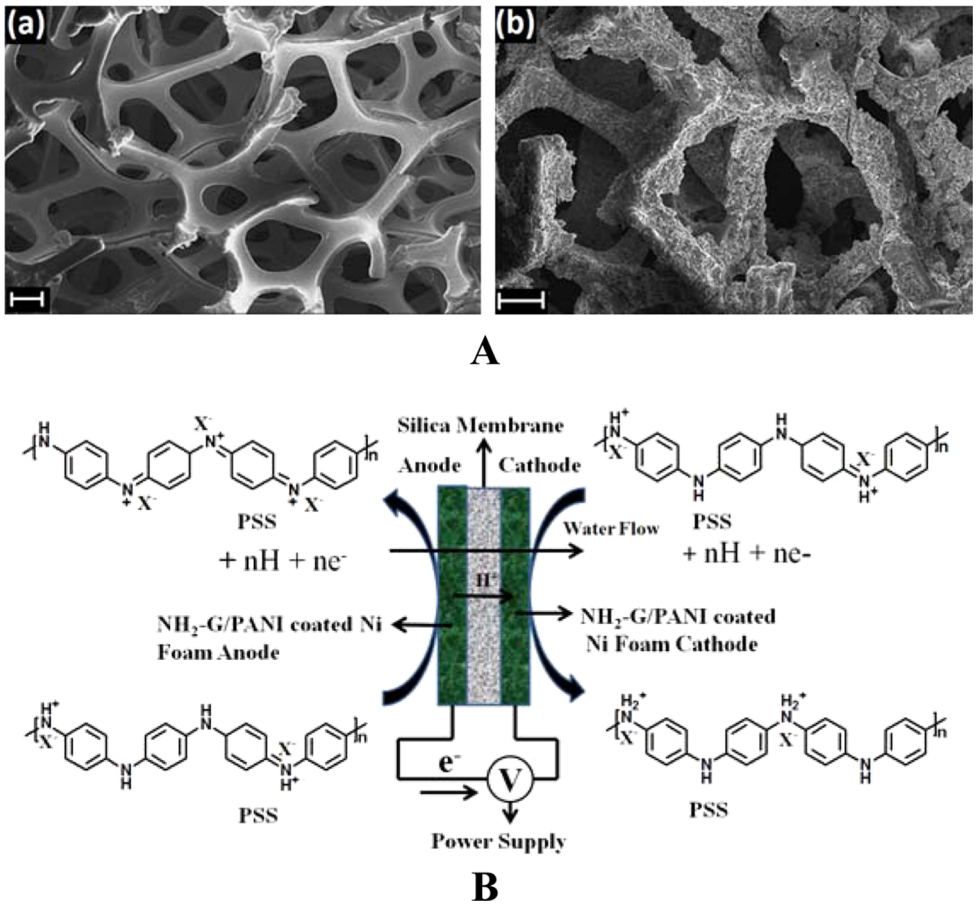

Figure 5. (A) SEM images of the nickel foam (a) before and (b) after coating of the electro-active NH_2-G/PANI-90.90 composite paste. (B) Schematics of the pump showing sandwich assembly and electrode reactions.

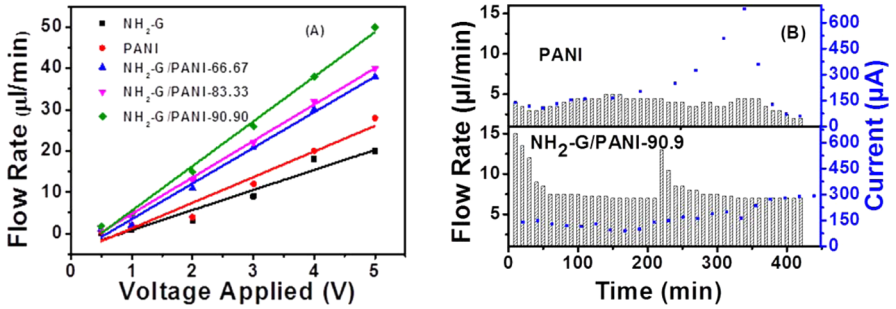

Figure 6. Electro-osmotic performance of the assembled pumps. (A) Dependence of flow rate on applied constant potential, the slope for NH_2-G = 5.3; PANI = 6.8; NH_2-G/PANI-66.67 = 9.1; NH_2-G/PANI-83.33 = 9.1; NH_2-G/PANI-90.90 = 11.3. (B) Life of the pump evaluated by continuous operation for 7 h at constant applied voltage of 2 V.

EOPs employing Ag/silica frit/Ag_2O[1] or silicon thin films.[7] The electro-osmotic flux of an Ag/silica frit/Ag_2O-based EOP[1] was measured at 130 μL min^{-1} cm^{-2} V^{-1}, while a flux of 86 mL min^{-1} cm^{-2} at an applied potential of 70 V was obtained with a thin-film based EOP assembled with silica coated aluminum anodic oxide membranes.[40] The EOP with the highest reported normalized flux per unit applied voltage of 2600 μL min^{-1} cm^{-2} V^{-1} was prepared with a 15 nm thick porous nanocrystalline silicon membrane.[7] Such an exceptionally high flux is the result of extremely low membrane thickness and trans-membrane resistance. However, as discussed below, the pressure developed by such pumps (stall pressure) and their efficiency can be rather low compared to the pump developed here. Further, unlike the other consumable electrodes that leak toxic ions, such as Ag/Ag_2O, the NH_2-G/PANI electrodes have added advantage of exceptionally stable electrode and flow rates until the full utilization of their columbic capacity. Their noncontaminating nature is especially attractive for analytical and medical applications. Finally, it may be noted that the flux depends largely on the hydraulic permeability and the zeta potential of the membrane/frit and can be increased by increasing its porosity and reducing its thickness. However, our focus is not on the optimization of the membrane, but on the development of the nongassing, long-lasting, stable, and consumable electrodes.

Lifetime of the Electro-osmotic Pump. The simple sandwich-type electro-osmotic pump assembled here has consumable electrodes. This means that the lifetime of the electrodes depends on the columbic capacity of both the anode

dx.doi.org/10.1021/am506766e | ACS Appl. Mater. Interfaces 2015, 7, 593−601

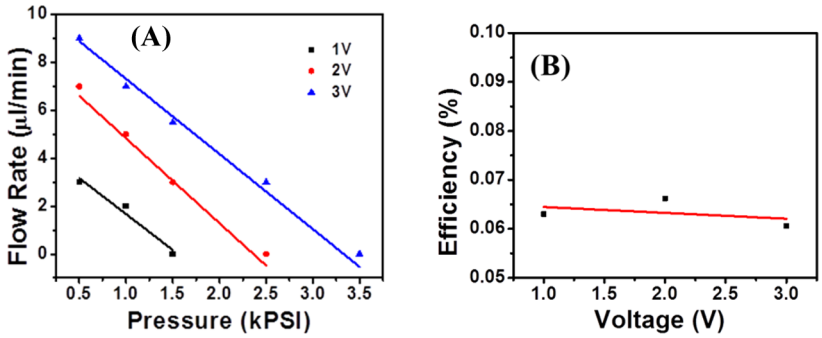

Figure 7. Electro-osmotic performance of the assembled pumps. (A) Dependence of flow rate on flow opposing pressure at different voltages. (B) Efficiency of the pump measured at different voltages.

and cathode. We determined the columbic capacity of the NH_2-G/PANI-90.9 electrode by discharging at constant potential. The anode and cathode were discharged at 0.8 and −0.2 V respectively vs Ag/AgCl in 20 mM phosphate buffer at pH 7. The resulting columbic capacity was 110 mC for the anode and 32 mC for the cathode. The discharge potentials were selected based on the cyclic voltammograms and these were well above and below the oxidation/reduction potential of PANI. EOPs assembled with either neat PANI or NH_2-G/PANI-90.9 electrodes were operated continuously for 7 h at a constant voltage of 2 V. The flow rates measured every 10 min are presented in Figure 6B. The average flow rates are 4.0 and 8.0 μL/min with PANI and NH_2-G/PANI-90.9, respectively. The flow rate with the NH_2-G/PANI-90.9 composite electrode is therefore double that obtained with neat PANI. Over 7 h, the neat PANI based electrode pumped 1.7 mL of water, which corresponds to ∼9000 water molecules per reacting electron. In comparison, the NH_2-G/PANI-90.9 electrode pumped 3.3 mL water which corresponds to ∼18000 water molecule per reacting electron. The analysis of Figure 6B reveals that the flow rate of PANI fluctuated around 4 ± 1 μL/min throughout the run, whereas with NH_2-G/PANI-90.9, with the exception of the initial cycle, the flow rate remained constant. The initial flow rate was 15 μL/min; this slowly decreased after a few runs to 8.0 μL/min and then remained constant at this value. This initial difference in change in the flow is explained on the basis of formation of different forms of PANI, i.e., pernigraniline and leucoemeraldine form at anode and cathode from emeraldine salt, respectively. Consider the characteristic general formula of PANI as $[(-B-NH-B-NH-),(-B-N{=}Q{=}N-)_{1-y}]_x$, in which B and Q represents the C_6H_4 rings in the benzenoid and quinonoid forms, respectively. Thus, PANI is basically poly(p-phenyleneimineamine)s, in which the neutral intrinsic redox states can vary from that of the fully oxidized pernigraniline (PNA, $y = 0$), to that of the fully reduced leucoemeraldine (LM, $y = 1$). The 50% intrinsically oxidized polymer has been termed emeraldine (EM, $y = 0.5$), often referred to as emeraldine base (EB), which is neutral. When doped (i.e., protonated with acid) in the present study by PSS, it is called emeraldine salt (ES) which has imine nitrogens protonated by an acid. Protonation helps to delocalize the otherwise trapped diiminoquinone−diaminobenzene state. Emeraldine base is regarded as the most useful form of polyaniline due to its high stability at room temperature and its high electrical conductivity upon doping with acid.[41] Leucoemeraldine and pernigraniline are poor conductors,[42] even when doped with acid. The higher initial value of flow rate is due to the easily released charge of the emeraldine salt form of PANI. As this charge is consumed, the emeraldine form converts by oxidation into a less conducting pernigraniline salt at the anode and by reduction to leucoemeraldine salt at the cathode, with the clean generation and consumption of protons. The pernigraniline salt and the leucoemeraldine salt are less conductive than the emeraldine form,[43] and hence, it consumes more potential than is used to flow water, leading to the decrease in flow rate observed. The high flow rate for NH_2-G/PANI-90.9 composite compare to neat PANI is observed by increase in conductivity of electrodes in the presence of graphene sheet in between the PANI chains which increases the utilization of actual potential applied to operate the pump. The graph for NH_2-G/PANI-90.9 in Figure 6B shows a sudden increase in the flow rate at 220 min. This is due to the pump being turned off overnight, which reaccumulated columbic capacity on resting. The flow rate was therefore higher in the initial run on restarting it the next day. Details of the electrode reaction and schematics of the assembled pump and the flow mechanism are presented in Figure 5B. From the figure it is clear that the columbic capacity of the electrode is reversible and that changing the polarity allows the pump to run for a maximum number of cycles. The overall flow rate (except initially) was within an error limit of ±10%. The plot of current versus time shown in Figure 6B for neat PANI and NH_2-G/PANI composite electrodes clearly reveals the role of graphene sheet in stabilization of electrodes. The continuous increase of current with time for the neat PANI indicates the slow leaching of PSS in water. It reached the maximum value at around 340 min and then suddenly decreased. The sudden decease may be owing to the complete exhaustion of the columbic capacity of the electrode as evident by a decrease in the flow rate. In the case of NH_2-G/PANI, the increase in current with time is very slow, suggesting effective stabilization of electrode by ionic cross-linking of PSS. These results clearly reveal the benefits of NH_2-G/PANI composite electrodes over neat PANI in electro-osmotic pumping.

Efficiency of the EOP. The ability of EOPs to provide the maximum stall pressure provided at the minimum applied voltage determines their applicability. The dependence of the flow rate on the flow-opposing pressure was analyzed by plotting the two against each other using eq 1 as follows:[44]

$$\frac{Q}{Q_{max}} = 1 - \frac{P}{P_{max}} \quad (1)$$

where Q is the flow rate and P the opposing pressure. The measured flow rates and pressures were respectively normalized to Q_{max}, the maximum flow rate at zero opposing pressure and P_{max}, the maximum pressure at zero flow rate.

dx.doi.org/10.1021/am506766e | ACS Appl. Mater. Interfaces 2015, 7, 593−601

Figure 7A shows the stall pressure measured for an EOP assembled with NH_2-G/PANI-90.9 at different voltages wherein no gas is produced. From the figure, it is clear that the stall pressure increases with the applied voltage. At a constant applied voltage of 1.0 V, this flow-through EOP gave 1.5 kPa pressure with no flow and 0.5 kPa at 3.0 μL/min. At 2.0 and 3.0 V the maximum stall pressures obtained were 2.5 and 3.5 kPa, respectively.

The stall pressure and flow rate can be used to calculate the thermodynamic efficiency (η) of the EOP. The thermodynamic efficiency (η) represents the hydraulic power generated over the total electrical power consumed and is calculated using eq 2,

$$\eta = \frac{1}{4}\frac{Q_{max}P_{max}}{IV_{app}} \quad (2)$$

where I is the current and V_{app} is the applied voltage.

Figure 7B shows the thermodynamic efficiency of the NH_2-G/PANI-90.9 EOP, the best one investigated here, which was calculated from the measured stall pressures and flow rates. The efficiency of this device was 0.065% and remained constant at different applied voltages varying only by ±0.005%. This value is higher than the efficiency reported for nonsilicon-based EOPs.[7] In the literature, experimental thermodynamic efficiencies lie in the range of 0.005−2.0%.[7,45,46] The efficiency of our device can be increased by optimizing the membrane and by using thermodynamically stable and kinetically fast electrodes.

CONCLUSIONS

In summary, we have successfully developed an efficient, nongassing, noncontaminating, and stable electro-osmotic pump with consumable PANI-wrapped NH_2-G electrodes. The miniature pump was assembled by sandwiching a silica frit (area ~0.28 cm^2) between two flow-through electrodes prepared by dip coating nickel foam with PANI-tethered NH_2-G. The performance of this EOP was tested at constant applied voltage and found to depend linearly on the voltage as well as on the composition of the electrodes. The normalized flow rates at a constant potential of 5 V was increased from 125.0 to 182.1 $\mu L\ min^{-1}\ cm^{-2}$ as the weight fraction of aniline was increased from 66.63 to 90.90%, but it declined thereafter, suggesting an optimal composition for the electrodes. The maximum flux per unit applied voltage obtained was 40.4 $\mu L\ min^{-1}\ cm^{-2}\ V^{-1}$, with NH_2-G/PANI-90.9 electrodes. EOPs assembled with neat PANI and NH_2-G/PANI-90.9 electrodes remained exceptionally stable until the exhaustion of the electrode charges lasting over 7 h of continuous operation. NH_2-G/PANI-90.9 electrodes delivered a flow rate of 8.0 μL/min at a constant applied voltage of 2 V, which is double that of the neat PANI electrodes. The maximum stall pressure at zero flow for the best EOP (NH_2-G/PANI-90.9 electrode) was 3.5 KPa at 3 V. The electrode characteristics make them suitable in a plethora of microfluidic and lab-on-a-chip applications.

AUTHOR INFORMATION

Corresponding Authors

*E-mail: nagarale@iitk.ac.in.
*E-mail: ashutos@iitk.ac.in.

Notes

The authors declare no competing financial interest.

ACKNOWLEDGMENTS

R.K.N. thanks the Department of Science & Technology (DST), Government of India, for Ramanujan Fellowship (SR/S2/RJN-18/2011) award and financial support, (grant no. SR/S3/CE/034/2013). This work was supported by the Department of Science and Technology, India.

REFERENCES

(1) Shin, W.; Lee, J. M.; Nagarale, R. K.; Shin, S. J.; Heller, A. A Miniature, Nongassing Electro-osmotic Pump Operating at 0.5 V. *J. Am. Chem. Soc.* **2011**, *133*, 2374−2377.
(2) Nagarale, R. K.; Heller, A.; Shin, W. A Stable Ag/Ceramic-Membrane/Ag_2O Electro-osmotic Pump Built with a Mesoporous Phosphosilicate-on-Silica Frit Membrane. *J. Electrochem. Soc.* **2012**, *159*, 14−17.
(3) Lakhotiya, H.; Mondal, K.; Nagarale, R. K.; Sharma, A. Low Voltage Non-Gassing Electro-Osmotic Pump with Zeta Potential Tuned Aluminosilicate Frits and Organic Dye Electrodes. *RSC Adv.* **2014**, *4*, 28814−28821.
(4) Shin, W.; Zhu, E.; Nagarale, R. K.; Kim, C. H.; Lee, J. M.; Shin, S. J.; Heller, A. Nafion-Coating of the Electrodes Improves the Flow-Stability of the Ag/SiO_2/Ag_2O Electro-osmotic Pump. *Anal. Chem.* **2011**, *83*, 5023−5025.
(5) Erlandsson, P. G.; Robinson, N. D. Electrolysis-Reducing Electrodes for Electrokinetic Devices. *Electrophoresis* **2011**, *32*, 784−790.
(6) Luft, G.; Kuhl, D.; Richter, G. J. Electro-osmotic Pump for Steady Regulated or Controlled Release Of Medicaments. *Biomed. Technol.* **1977**, *22*, 169−173.
(7) Snyder, J. L.; Getpreecharsawas, J.; Fang, D. Z.; Gaborski, T. R.; Striemer, C. C.; Fauchet, P. M.; Borkholder, D. A.; McGrath, J. L. High-Performance, Low-Voltage Electro-osmotic Pumps with Molecularly Thin Silicon Nanomembranes. *Proc. Natl. Acad. Sci. U.S.A.* **2013**, *110*, 18425−18430.
(8) Tsai, N.-C.; Sue, C.-Y. Review of MEMS-Based Drug Delivery and Dosing Systems. *Sens. Actuators, A* **2007**, *134*, 555−564.
(9) Uhlig, E. L. P.; Graydon, W. F.; Zingg, W. The Electro-Osmotic Actuation of Implantable Insulin Micropumps. *J. Biomed. Mater. Res.* **1983**, *17*, 931−943.
(10) Wang, X.; Wang, S.; Gendhar, B.; Cheng, C.; Byun, C. K.; Li, G.; Zhao, M.; Liu, S. Electro-osmotic Pumps for Microflow Analysis. *TrAC, Trends Anal. Chem.* **2009**, *28*, 64−74.
(11) Huang, C.-C.; Bazant, M. Z.; Thorsen, T. Ultrafast High-Pressure AC Electro-Osmotic Pumps for Portable Biomedical Microfluidics. *Lab Chip* **2009**, *10*, 80−85.
(12) Kutter, J. r. P.; Jacobson, S. C.; Ramsey, J. M. Integrated Microchip Device with Electrokinetically Controlled Solvent Mixing for Isocratic and Gradient Elution in Micellar Electrokinetic Chromatography. *Anal. Chem.* **1997**, *69*, 5165−5171.
(13) Hadd, A. G.; Raymond, D. E.; Halliwell, J. W.; Jacobson, S. C.; Ramsey, J. M. Microchip Device for Performing Enzyme Assays. *Anal. Chem.* **1997**, *69*, 3407−3412.
(14) Prakash, P.; Grissom, M. D.; Rahn, C. D.; Zydney, A. L. Development of an Electro-osmotic Pump for High Performance Actuation. *J. Membr. Sci.* **2006**, *286*, 153−160.
(15) Geim, A. K.; Novoselov, K. S. The Rise of Graphene. *Nat. Mater.* **2007**, *6*, 183−191.
(16) Dikin, D. A.; Stankovich, S.; Zimney, E. J.; Piner, R. D.; Dommett, G. H. B.; Evmenenko, G.; Nguyen, S. T.; Ruoff, R. S. Preparation and Characterization of Graphene Oxide Paper. *Nature* **2007**, *448*, 457−460.
(17) Gomez-Navarro, C.; Weitz, R. T.; Bittner, A. M.; Scolari, M.; Mews, A.; Burghard, M.; Kern, K. Electronic Transport Properties of Individual Chemically Reduced Graphene Oxide Sheets. *Nano Lett.* **2007**, *7*, 3499−3503.
(18) Novoselov, K. S.; Geim, A. K.; Morozov, S. V.; Jiang, D.; Zhang, Y.; Dubonos, S. V.; Grigorieva, I. V.; Firsov, A. A. Electric Field Effect in Atomically Thin Carbon Films. *Science* **2004**, *306*, 666−669.

(19) Stankovich, S.; Dikin, D. A.; Dommett, G. H. B.; Kohlhaas, K. M.; Zimney, E. J.; Stach, E. A.; Piner, R. D.; Nguyen, S. T.; Ruoff, R. S. Graphene-Based Composite Materials. *Nature* **2006**, *442*, 282−286.
(20) Avouris, P.; Chen, Z.; Perebeinos, V. Carbon-Based Electronics. *Nat. Nano* **2007**, *2*, 605−615.
(21) Zhang, K.; Zhang, L. L.; Zhao, X. S.; Wu, J. Graphene/Polyaniline Nanofiber Composites as Supercapacitor Electrodes. *Chem. Mater.* **2010**, *22*, 1392−1401.
(22) Li, Z. F.; Zhang, H. Y.; Liu, Q.; Liu, Y. D.; Stanciu, L.; Xie, J. Novel Pyrolyzed Polyaniline-Grafted Silicon Nanoparticles Encapsulated in Graphene Sheets As Li-Ion Battery Anodes. *ACS Appl. Mater. Interfaces* **2014**, *6*, 5996−6002.
(23) Wang, G.; Xing, W.; Zhuo, S. The Production of Polyaniline/Graphene Hybrids for Use as a Counter Electrode in Dye-Sensitized Solar Cells. *Electrochim. Acta* **2012**, *66*, 151−157.
(24) Sun, W.; Peng, T.; Liu, Y.; Xu, S.; Yuan, J.; Guo, S.; Zhao, X.-Z. Hierarchically Porous Hybrids of Polyaniline Nanoparticles Anchored on Reduced Graphene Oxide Sheets as Counter Electrodes for Dye-Sensitized Solar Cells. *J. Mater. Chem. A* **2013**, *1*, 2762−2768.
(25) Yong, Y.-C.; Dong, X.-C.; Chan-Park, M. B.; Song, H.; Chen, P. Macroporous and Monolithic Anode Based on Polyaniline Hybridized Three-Dimensional Graphene for High-Performance Microbial Fuel Cells. *ACS Nano* **2012**, *6*, 2394−2400.
(26) Al-Mashat, L.; Shin, K.; Kalantar-zadeh, K.; Plessis, J. D.; Han, S. H.; Kojima, R. W.; Kaner, R. B.; Li, D.; Gou, X.; Ippolito, S. J.; Wlodarski, W. Graphene/Polyaniline Nanocomposite for Hydrogen Sensing. *J. Phys. Chem. C* **2010**, *114*, 16168−16173.
(27) Zhao, L.; Zhao, L.; Xu, Y.; Qiu, T.; Zhi, L.; Shi, G. Polyaniline Electrochromic Devices with Transparent Graphene Electrodes. *Electrochim. Acta* **2009**, *55*, 491−497.
(28) Chang, C.-H.; Huang, T.-C.; Peng, C.-W.; Yeh, T.-C.; Lu, H.-I.; Hung, W.-I.; Weng, C.-J.; Yang, T.-I.; Yeh, J.-M. Novel Anticorrosion Coatings Prepared from Polyaniline/Graphene Composites. *Carbon* **2012**, *50*, 5044−5051.
(29) Yan, X.; Chen, J.; Yang, J.; Xue, Q.; Miele, P. Fabrication of Free-Standing, Electrochemically Active, and Biocompatible Graphene Oxide-Polyaniline and Graphene-Polyaniline Hybrid Papers. *ACS Appl. Mater. Interfaces* **2010**, *2*, 2521−2529.
(30) Yao, S.; Hertzog, D. E.; Zeng, S.; Mikkelsen, J. C., Jr.; Santiago, J. G. Porous Glass Electro-osmotic Pumps: Design and Experiments. *J. Colloid Interface Sci.* **2003**, *268*, 143−153.
(31) Hummers, W. S.; Offeman, R. E. Preparation of Graphitic Oxide. *J. Am. Chem. Soc.* **1958**, *80*, 1339−1339.
(32) Lai, L.; Chen, L.; Zhan, D.; Sun, L.; Liu, J.; Lim, S. H.; Poh, C. K.; Shen, Z.; Lin, J. One-Step Synthesis of NH_2−Graphene from In Situ Graphene−Oxide Reduction and its Improved Electrochemical Properties. *Carbon* **2011**, *49*, 3250−3257.
(33) Ray, A.; Asturias, G. E.; Kershner, D. L.; Richter, A. F.; MacDiarmid, A. G.; Epstein, A. J. Polyaniline: Doping, Structure, and Derivatives. *Synth. Met.* **1989**, *29*, 141−150.
(34) Cancado, L. G.; Pimenta, M. A.; Neves, B. R. A.; Dantas, M. S. S.; Jorio, A. Influence of the Atomic Structure on the Raman Spectra of Graphite Edges. *Phys. Rev. Lett.* **2004**, *93*, 247401.
(35) Ferrari, A. C.; Robertson, J. Interpretation of Raman Spectra of Disordered and Amorphous Carbon. *Phys. Rev. B* **2000**, *61*, 14095−14107.
(36) Compton, O. C.; Dikin, D. A.; Putz, K. W.; Brinson, L. C.; Nguyen, S. T. Electrically Conductive "Alkylated" Graphene Paper via Chemical Reduction of Amine-Functionalized Graphene Oxide Paper. *Adv. Mater.* **2010**, *22*, 892−896.
(37) Xu, J.; Wang, K.; Zu, S.-Z.; Han, B.-H.; Wei, Z. Hierarchical Nanocomposites of Polyaniline Nanowire Arrays on Graphene Oxide Sheets with Synergistic Effect for Energy Storage. *ACS Nano* **2010**, *4*, 5019−5026.
(38) Zeng, S.; Chen, C.-H.; Mikkelsen, J. C., Jr; Santiago, J. G. Fabrication and Characterization of Electro-osmotic Micropumps. *Sens. Actuators, B* **2001**, *79*, 107−114.
(39) Brask, A.; Kutter, J. P.; Bruus, H. Long-Term Stable Electro-osmotic Pump with Ion Exchange Membranes. *Lab Chip* **2005**, *5*, 730−738.
(40) Miao, J. Y.; Xu, Z. L.; Zhang, X. Y.; Wang, N.; Yang, Z. Y.; Sheng, P. Micropumps Based on the Enhanced Electro-osmotic Effect of Aluminum Oxide Membranes. *Adv. Mater.* **2007**, *19*, 4234−4237.
(41) Kang, E. T.; Neoh, K. G.; Tan, K. L. Polyaniline: A Polymer with Many Interesting Intrinsic Redox States. *Prog. Polym. Sci.* **1998**, *23*, 277−324.
(42) Focke, W. W.; Wnek, G. E.; Wei, Y. Influence of Oxidation State, pH, and Counterion on the Conductivity of Polyaniline. *J. Phys. Chem.* **1987**, *91*, 5813−5818.
(43) Anthony Smith, J.; Josowicz, M.; Janata, J. Gold-Polyaniline Composite Part I. Moving Electrochemical Interface. *Phys. Chem. Chem. Phys.* **2005**, *7*, 3614−3618.
(44) Osterle, J. F. Electrokinetic Energy Conversion. *J. Appl. Mech.* **1964**, *31*, 161−164.
(45) Shuhuai, Y.; Myers, A. M.; Posner, J. D.; Rose, K. A.; Santiago, J. G. Electro-osmotic Pumps Fabricated from Porous Silicon Membranes. *J. Microelectromech. Syst.* **2006**, *15*, 717−728.
(46) Wang, C.; Wang, L.; Zhu, X.; Wang, Y.; Xue, J. Low-Voltage Electro-osmotic Pumps Fabricated From Track-Etched Polymer Membranes. *Lab Chip* **2012**, *12*, 1710−1716.